DESDE 2013
https://repository.uaeh.edu.mx/revistas/index.php/icbi/issue/archive
Pädi Boletín Científico de Ciencias Básicas e Ingenierías del ICBI

ISSN: 2007-6363

Publicación Semestral Pädi Vol. 14 No. Especial 2 (2026) 190-195

Influence of Spin–Orbit Coupling on the Electronic Structure of $MnBi_2Te_4$ and Bi_2Te_3
Influencia del acoplamiento espín–órbita en la estructura electrónica de $MnBi_2Te_4$ y Bi_2Te_3

R. Flores-Cruz[a], J.B Ortega-Lazcano[b], K.A Martínez-Legaria[a,c], Ventura Rodríguez-Lugo[a,*]

[a]*Universidad Autónoma del Estado de Hidalgo - Área Académica de Ciencias de la Tierra y Materiales, Instituto de Ciencias Básicas e Ingeniería, Mineral de la Reforma Carretera Pachuca-Tulancingo Km. 4.5, 42184. Hidalgo, México.*
[b]*Instituto Tecnológico Nacional, campus Pachuca, Carretera México - Pachuca Km. 87.5, C.P. 42080, Colonia Venta Prieta, Pachuca de Soto, Hidalgo, México.*
[c]*Universidad Tecnológica de Tecámac - Academia de Nanotecnología, División de Procesos Industriales, Carretera Federal México-Pachuca km 37.5, Colonia Sierra Hermosa, San Martín Azcatepec, Tecámac, C.P. 55740, Estado de México, México.*

Abstract
A theoretical study was carried out on Bi_2Te_3 and $MnBi_2Te_4$ systems using the SIESTA computational code, to establish an adequate methodology for the simulations in this program. In order to determine the best parameters to perform the simulations, two types of pseudopotentials were used, using the local density approximation (LDA) and using the generalized gradient approximation (GGA), considering both the non-relativistic and the fully relativistic cases. In addition, calculations were also performed using the DFT+U and spin–orbit coupling (SOC) corrections. The band gaps obtained for the MnBi2Te4 system with LDA and GGA were 0.17 eV and 0.21 eV, respectively, while the band gaps of the Bi2Te3 system with LDA and GGA were 0.17 eV and 0.30 eV, respectively. This work shows the importance of including the effects of the spin–orbit coupling in the calculations of the electronic properties of this type of materials and compares the results with those of other investigations.

Keywords: SIESTA, electronic properties, topological insulator, simulation.

Resumen

Se llevó a cabo un estudio teórico sobre los sistemas Bi_2Te_3 y $MnBi_2Te_4$ utilizando el código computacional SIESTA, con el fin de establecer una metodología adecuada para las simulaciones en este programa. Para determinar los mejores parámetros para realizar las simulaciones, se utilizaron dos tipos de pseudopotenciales, utilizando la aproximación de densidad local (LDA) y la aproximación de gradiente generalizado (GGA), considerando tanto los casos no relativistas como los totalmente relativistas. Además, también se realizaron cálculos utilizando las correcciones DFT+U y de acoplamiento spin-órbita (SOC). Las bandas prohibidas obtenidas para el sistema $MnBi_2Te_4$ con LDA y GGA fueron de 0,17 eV y 0,21 eV, respectivamente, mientras que las bandas prohibidas del sistema Bi_2Te_3 con LDA y GGA fueron de 0,17 eV y 0,30 eV, respectivamente. Este trabajo muestra la importancia de incluir los efectos del acoplamiento spin-órbita en los cálculos de las propiedades electrónicas de este tipo de materiales y también compara los resultados con los de otras investigaciones.

Palabras Clave: SIESTA, propiedades electrónicas, aislante topológico, simulación.

1. Introduction

Condensed-matter physics focuses on understanding and classifying the different states and properties of matter. Some phases can be understood with the Landau´s approach, however, nowadays topological ordering can be used to identify the different phases of matter more clearly (Hasan y Kane, 2010; Thouless et al., 1982). In agreement with (Li et al., 2023), topological ordering was made possible by the discovery of the quantum Hall effect, in which the conductance is quantized and is a manifestation of the quantum effect on a macroscopic scale. An example of this topological phase of the matter is a topological insulator (TI), which is a new class of material that acts as an insulator in bulk while its surface is metallic. Sharma et al, (2019) explained that in these materials, the surface states are protected by a nontrivial topology, that arises from the interaction of spin–orbit coupling (SOC) and time-reversal symmetry. The two-dimensional (2D) topological insulator has gap-less states protected by time-reversal symmetry, while the three-dimensional (3D)

*Autor para la correspondencia: ventura.rl65@gmail.com
Correo electrónico: fl335558@uaeh.edu.mx (Rommel Flores Cruz) Jesus.ol@pachuca.tecnm (Jesús Benjamín Ortega Lazcano), kev2315@outlook.com (Kevin Alejandro Martínez Legaria), venturar@uaeh.edu.mx (Ventura Rodríguez Lugo)

Historial del manuscrito: recibido el 06/03/2026, última versión-revisada recibida el 11/03/2026, aceptado el 12/03/2026, publicado el 06/04/2026. **DOI:** https://doi.org/10.29057/icbi.v14iEspecial2.17123

topological insulator has an odd number of relativistic Dirac Fermions (Hasan y Kane, 2010; Chen et al., 2009).

(Lee et al., 2013; Li et al., 2019) discovered the material $MnBi_2Te_4$ or MBT. It has a rhombohedral crystalline structure with lattice parameters a = 4.334 Å and c = 40.91 Å. The atoms in each structure are Mn, Bi and Te, which are stacked one on top of the other in the Te-Bi-Te-Mn-Te-Bi-Te configuration. A slice of this material contains a septuple layer, which is kept together by van Der Waals bonds. In addition, each MBT crystalline structure contains 21 atoms in the aforementioned configuration, which also belongs to the $R\bar{3}m$ space group and can be said to be very similar to Bi_2Te_3 but with an intercalated layer of Mn-Te. The valence states of the atoms of the Bi_2Te_3 atoms are Mn^{+3} and Bi^{+2}, which are energetically unfavorable states, while the valence states of the atoms of the MBT are Mn^{+2}, Bi^{+3} and Te^{-2}. The electron configuration of Mn indicates, according to Hund's rule, that since the 4s orbital runs out of electrons, then the next most energetic orbital left is the d, with all the electron spins pointing in the same direction and thus yielding a magnetic moment of $5\mu_B$.

The topological insulators have potential applications in dissipation-less transport, photodetectors, magnetic devices, field-effect transistors (Tian et al., 2017), spintronics and quantum computation (Wang et al., 2017). The inclusion of effects such as spin–orbit coupling in the calculations on these materials has been observed previously, in fact a gap in Γ of 0.37 eV has been obtained for the BT system without SOC (Larson et al., 2000) and LDA calculations on this system indicate a direct band gap of 0.05 eV (Michiardi et al., 2014). Further evidence of the importance of considering spin–orbit coupling, not only in the values but also in the behavior exhibited energy bands, is provided by other theoretical works that have compared the values obtained for the band gap with experimental results, which obtained values of 0.31 eV (Lawal y Shaari, 2017) and 0.28 eV (Soler et al., 2002) without SOC, and 0.13 (Lawal y Shaari, 2017) with SOC. The calculation conditions for the MBT vary in comparison to those of its precursor BT, inasmuch the only way to obtain good results with the SIESTA code is by implementing SOC, because this material contains manganese atoms, for which the DFT+U correction is normally used, as well as atoms with a strong spin–orbit coupling such as bismuth and tellurium.

In the present work, a theoretical study was carried out using the density functional theory (DFT) as implemented in the computational code Spanish Initiative for Electronic Simulations with Thousands of Atoms (SIESTA), in order to determine how the implementation of corrections such as DFT +U or the effects of spin–orbit coupling affects the calculations of energy bands in the topological insulators Bi_2Te_3 (BT) and $MnBi_2Te_4$ (MBT). To achieve this, the simplest systems that could be constructed from these materials were analyzed. The simplest repetitive units of a monolayer, which have the atoms stacked one on top of the other in the following ways: Te-Bi-Te-Bi -Te and Te-Bi-Te-Mn-Te-Bi-Te, are a quintuple layer and a septuple layer, respectively. The electronic properties of the Bi_2Te_3 system were obtained following the K-Γ-M route in order to establish how the band gap is affected including the aforementioned effects. For the case of $MnBi_2Te_4$, the same analysis was performed with the high symmetry points corresponding to a two-dimensional lattice and then the calculations were repeated for a larger 3x3 system with the parameters that were considered most effective to obtain better results in the systems.

2. Methodology and computational details

The calculations were performed using the SIESTA DZP basis set computational code (Soler et al., 2002), which is based on the density functional theory (DFT). A meshcutoff of 500 Ry and a k point mesh 9x9x1 were employed. Relativistic pseudopotentials in the local density approximation (LDA) and in the generalized gradient approximation (GGA) were utilized, and the DFT+U method (Dudarev et al., 2002) was used to treat the localized 3d orbitals of the manganese atom. The value of U = 4 eV was selected based consistently with the value used by other simulation programs (Li et al., 2019). Monolayer systems, quintuple and septuple layers, a single row of atoms, and a larger 3x3 system for MBT were studied, with a tolerance for the structural relaxation of 0.001 eV/Å, a convergence of $1x10^{-5}$ and a vacuum thickness in the case of monolayers 15 Å. Finally, the calculations includes SOC effect.

3. Results and discussion

3.1. Bi_2Te_3 and $MnBi_2Te_4$ systems

Figure 1 shows the band structures obtained from the simulation with LDA (blue) and GGA (red) pseudopotentials. For this case, all the calculations were done without including DFT+U or the spin–orbit correction. It can be seen in a) and b) that, by ignoring those effects, an inaccuracy at the Fermi level arises near the Γ point, with both the LDA and the GGA pseudopotentials, which shows that the valence bands contain some energies greater than those of the Fermi level, something that is contradictory according to the results obtained in previous works (Li et al., 2019). The graphs c) and d) show the bands corresponding to the BT system, in which the Fermi level adequately separates the valence and conduction bands and denotes a semiconducting manner like a TI used to have. No considerable differences are observed between the use of LDA or GGA pseudopotentials in terms of the behavior of the energy bands. However, there is a difference in the extreme energy values of the BT system close to the Γ points, depending on the use of an LDA pseudopotential c) or a GGA pseudopotential d), with differences between the valence and conduction bands at point Γ of approximately 0.66 eV and 0.76 eV, respectively.

3.2. $MnBi_2Te_4$ including DFT+U

In this case, a value of U = 4 eV was included to try to correct the inaccuracy found in the Fermi level shown in the previous case (Figure 1), this value for U was established in agreement with previous works, where a value of U = 4 eV was used for Mn (Li et al., 2019) due to the presence of its localized 3d electrons, generates strong electronic correlations, these states can significantly affect the band dispersion near the Fermi level. Figure 2 (a and b) shows the two band graphs obtained including this parameter. As can be seen, including this correction does not have sufficient effect on the energy bands, resulting in the same inaccuracy of the Fermi level, but

making the energy bands more pronounced close to the Γ point. Ignoring the imprecision of the Fermi level, the gap that separates the valence bands from the conduction bands above the Γ point is 0.6 eV for LDA and 0.75 eV for GGA, which only serve as a reference to denote the separation that exists between the conduction and valence bands with both pseudopotentials, but do not describe a real gap, because of the considerable differences between both pseudopotentials. In Figure 2a a peak can be seen over the Γ point, while a trough can be seen over the same point in Figure 2b. In addition, the LDA case does not show a clear gap, which would seem to indicate that it tends toward metallic behaviour; on the contrary a clear separation between the conduction and valence bands is observed for the GGA.

3.3. Bi_2Te_3 and $MnBi_2Te_4$ including SOC

Spin–orbit coupling was incorporated in the calculations in order to properly account for the strong relativistic effects associated with heavy elements such as Bi and Te atoms which plays a fundamental role in the electronic structure of topological insulators because of the band inversion near the Γ point, which is a characteristic of TI. separation between the valence and conduction bands for the MBT systems becomes clearer when the SOC effects are included, showing a bandgap between both valence and conduction bands. The gap is larger in the Γ point for the LDA case (0.34 eV) than for the GGA case (0.22 eV), showing a peak and a trough respectively, which indicate a direct gap for GGA and an indirect gap for LDA (0.17 eV). In the case of the BT system, the results also vary considerably by including the spin–orbit coupling effects and by the usage of the LDA or GGA pseudopotentials. At the first high symmetry point, the energy gaps between the valence and conduction bands with LDA and GGA are 0.27 eV and 0.36 eV, respectively, both of which are considerably lower than those obtained when spin–orbit coupling was not considered. Figure 3 illustrates that incorporating spin–orbit coupling (SOC) effects into the calculations corrects inaccuracies at the Fermi level and clearly defines the gap separating the valence and conduction bands in these materials.

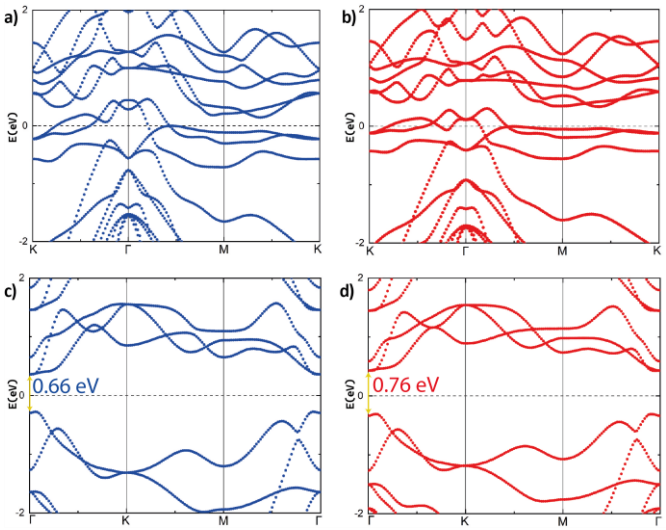

Figure 1: Band structures of the MBT system with (a, b) without corrections and band structures of the BT system without corrections (c, d). The blue and red colors correspond to LDA and GGA pseudopotentials, respectively. The Fermi energy was set to 0.

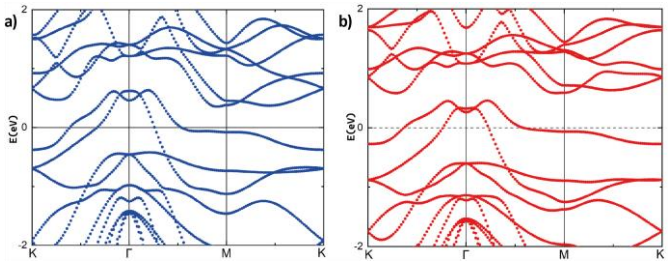

Figure 2: Band structures of the MBT system including U= 4eV: a) LDA, b) GGA. The Fermi energy was set to 0.

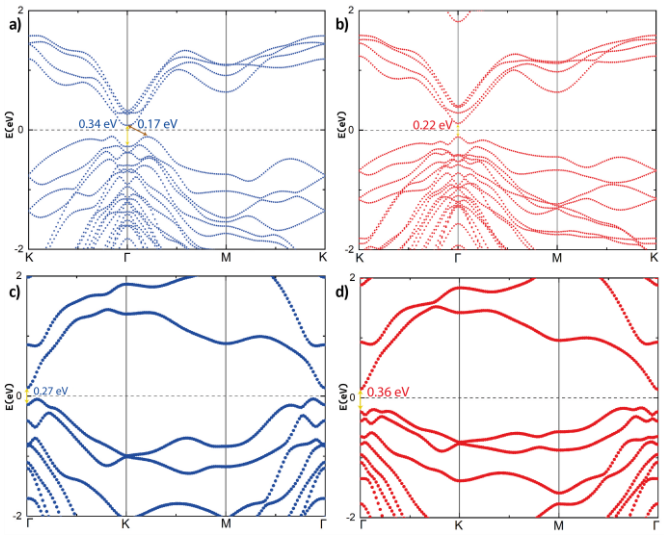

Figure 3: Band structures of the MBT (a,b) and BT (c,d) systems including SOC. The Fermi energy was set to 0.

In Figure 4 the bands of the BT system are shown following the K-Γ-M path to determine the effects of the corrections implemented on the band gap. In the Γ point the BT system has a gap of 0.64 eV with LDA and a gap of 0.75 eV with GGA, in agreement with the results shown above. When the effects of the SOC are included, the behavior of the energy bands is considerably modified, leaving with LDA a gap over Γ of 0.27 eV and an indirect gap of 0.17 eV, whereas with GGA the gap over Γ is 0.36 eV and there is an indirect gap of 0.30 eV. 4 eV value is employed to describe the 3d orbitals of the Mn atoms.

According to the results obtained for the MBT system, the electronic structure is strongly influenced by the presence of Mn atoms and the inclusion of spin–orbit coupling. MBT is a magnetic topological insulator in which the localized Mn 3d states introduce magnetic exchange interactions. When spin–orbit coupling is considered, these interactions significantly modify the band dispersion near the Fermi level and contribute to the formation of the bandgap and when SOC effects are not considered, the electronic properties are imprecise.

Based on Li et al., (2019) previous research, the Fermi level should be exactly halfway between the valence and conduction bands, without overlapping at all with the

conduction band. Furthermore, the behavior of the electronic bands is inaccurate when only the LDA pseudopotential is used, something that does not improve even when the Hubbard value of U = 4 eV is included. The best results for the MBT system were obtained when spin–orbit coupling was included in the calculations, for both LDA and GGA pseudopotentials are used. However, the GGA pseudopotential provided a band behavior that was quite good, even without including DFT+U or SOC, but the results contain inaccuracies in the obtained Fermi level values, as it is exceeded by the valence bands, which should not occur. Even when SOC is included, the LDA and GGA simulations show slight differences in the results, noticeable at the high symmetry point Γ, where LDA has a trough and GGA has a peak, and for the latter, a direct gap would be present.

The BT system shows some differences depending if the calculations are performed with or without considering spin–orbit coupling; however, it does not have the same issue noted in the MBT systems, specifically regarding the Fermi level. In this case, the Fermi level perfectly separates the valence bands from the conduction bands, indicating semiconductor behavior, property observed in topological insulators. This means that without SOC, the results for LDA and GGA are good and quite similar, with the only noticeable difference being the proximity between the valence and conduction bands at the Γ point. However, based on behavior observed in Li et al., (2019), the bands without SOC are not very much alike, being more clustered than expected.

Once SOC is included in the calculations for LDA and GGA, the bands are more separated and resemble the published results more closely, achieving better outcomes when using the GGA pseudopotential, as it better describes the behavior of the bands. This can be seen in the valence band closest to the Γ point.

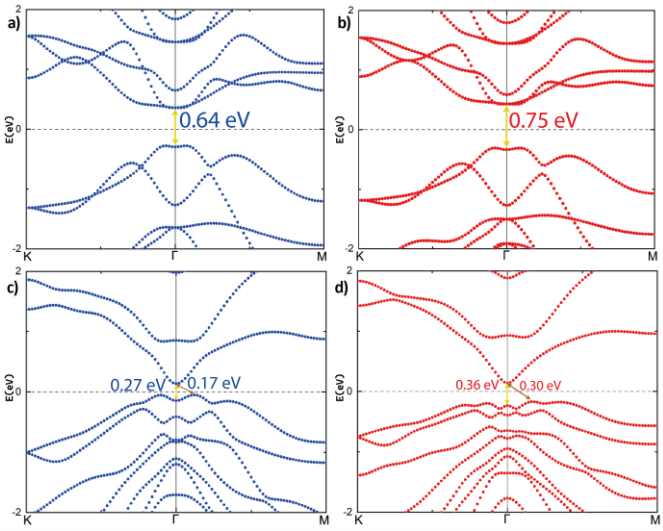

Figure 4: Band structures of the BT system a) LDA and b) GGA, without SOC, c) LDA and d) GGA, with SOC. The Fermi energy was set to 0.

3.4. MBT 3x3 system with SOC

A 3x3 supercell containing a total of 63 atoms was created to analyze the behaviour of energy bands when spin–orbit coupling (SOC) is implemented in calculations for larger systems. This approach aimed to determine whether the properties observed in smaller systems are preserved or if the inclusion of a greater number of atoms introduces any inaccuracies in the calculations. The results obtained by implementing SOC in the MBT 3x3 system using LDA and GGA pseudopotentials are shown in Figure 5. For the LDA pseudopotential, an indirect band gap of 0.17 eV was observed. On the other hand, the GGA pseudopotential displayed a direct band gap of 0.21 eV, a value very close to that obtained in previous calculations. These findings indicate that, despite the increased system size, the band gap values obtained with SOC remain consistent with earlier results, demonstrating the reliability of both pseudopotentials for larger systems.

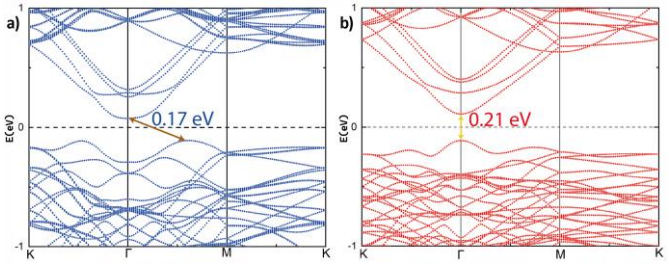

Figure 5: Band structures of 3x3 MBT system. a) LDA pseudopotential and b) GGA pseudopotential.

According to the obtained results, the most appropriate methodology for the SIESTA calculations for these topological insulators is the one that considers the effects of spin–orbit coupling. In this work, values of 0.17 and 0.22 eV for the bandgap of single-layer MBT were obtained, for LDA+SOC and GGA+SOC, respectively; those values are smaller than the ones reported by other research groups, which are in a range of 0.3 to 0.7 eV considering in each case the LDA/GGA pseudopotential nature, the monolayer configuration, and SOC interactions in addition to the magnetic intrinsic properties of Mn and the basis set of SIESTA that was used (Li et al., 2023) This suggests that actually, the inclusion of SOC affect directly in the electronic properties. This gap closing behaviour, when SOC is included, can be observed in other works and even when implemented in the simulation of other materials (Li et al., 2019; Li et al., 2023; Zhang et al., 2009). Figure 1, which corresponds to the case where no correction is implemented, shows a difference at point Γ regarding the implementation of a LDA or GGA pseudopotential, with the former presenting a possible direct gap and the latter an indirect gap. This behaviour on the nature of the bandgap is maintained when DFT+U is included in the calculations, but it reverses when SOC is considered. The above reversal on the bandgaps was confirmed by performing calculations, using both pseudopotentials with SOC, on a larger system, a 3x3 supercell, in which the bandgap for the GGA case went from 0.22 eV to 0.21 eV.

The results obtained for the BT system were good, regarding the behaviour of the energy bands and the location of the Fermi level, which clearly separated the valence bands from the conduction bands and exhibited the insulating behavior according to the literature. When SOC is considered, the behaviour of the energy bands is more similar to that shown in previous works (Zhou y Wang, 2015), but the omission of

SOC yielded gaps of 0.66 eV for LDA and 0.76 eV for GGA, which are considerably higher than those previously reported consequence of how the calculation parameters like cutoff and mesh and the pseudopotentials were set-up: up to 0.12 eV and 0.28 eV, with and without SOC, respectively (Aliabad y Kheirabadi, 2013). The gap for the BT in this work is, thus, not closed enough, with the LDA+SOC case yielding the value closest to the published references (Aliabad y Kheirabadi, 2013). Table 1 summarizes the results obtained, along with some results recovered from other publications.

These results are evidence that SOC calculations underestimate the energy band between the valence and conduction bands, resulting in a lower value than that which has been calculated in other investigations, as seen in Table 1. However, despite these values correspond to an insulating state which means that the insulating nature of these materials is preserved. The band gap that is closest to the one presented in the current research is 0.32 eV (Otrokov et al., 2019), which is practically double than calculated. In works where only DFT+U is included, the band gap is higher than that obtained when SOC is included, this is because the inclusion of SOC in the calculations further underestimates the energy gap. Something similar happens for the BT System, but unlike the MBT System, the calculated band gaps are energetically larger than those of the references (Larson et al., 2000; Fang et al., 2019), with the one calculated with LDA being the closest.

Table 1: Band gap values obtained in the current work and in previous works. Rel (Relativistic), Spin–Orbit Coupling (SOC).

System	Pseudopotential	Correction implemented	Band gap (eV)
This work			
MBT	LDA	-	-
MBT	LDA	DFT+U	-
MBT	LDA-Rel	SOC	0.17
MBT	GGA	-	-
MBT	GGA	DFT+U	-
MBT	GGA-Rel	SOC	0.22
BT	LDA	-	0.66
BT	LDA-Rel	SOC	0.17
BT	GGA	-	0.76
BT	GGA-Rel	SOC	0.30
MBT 3x3	LDA-Rel	SOC	0.17
MBT 3x3	GGA-Rel	SOC	0.21
Previous works			
MBT	GGA	SOC, DFT-U	0.32 (15)
MBT	GGA	DFT-U	0.70 (11)
MBT	GGA	DFT-U	0.55 (20)
MBT	-	-	0.052 (5)
BT	LDA	LAPW method	0.11 (4,14)
BT	GGA	LAPW method	0.13 (8,10)
BT	GGA	LAPW method	0.17 (4.7)

4. Conclusion

According to the obtained results, the implementation of SOC in the calculations for this type of materials, greatly improves the quality of those results, because without SOC, the electronic structure near the Fermi level is not accurately reproduced, leading to incorrect band dispersion and unrealistic band gap values, also, the type of pseudopotential employed is important due to the small variations between LDA and GGA can modify the band dispersion and even change the nature of the bandgap. The GGA pseudopotential effectively describes the behavior of the bands even without corrections, but it has inaccuracies in calculating the Fermi level, when using DFT+U in the calculations with a value of U = 4 eV, which has been used in other programs like VASP or Atomistix Toolkit. The comparison between the BT and MBT systems is reasonable because the systems only differ by a layer of Mn and Te, and because it allows for an understanding of whether the inaccuracy of the Fermi level is due to the manganese atom. The inclusion of GGA+U should be sufficient to correct the 3d orbitals of manganese and thus achieve good results. However, our findings in this paper suggest that the effects of the Bi and Te atoms are too significant to ignore SOC using the SIESTA code, and that the inclusion of the Mn atom produces underestimations on the band gap, making the results for the BT system more consistent with previous works. Thus, it is concluded that with SIESTA, good approximations for the study of the topological insulators BT and MBT can be obtained, but since the SOC must be included in the calculations, it is likely that smaller energy gaps will be obtained. Finally, the results paper leads to include the use of more advanced exchange-correlation functionals, such as hybrid functionals or GW methods, in order to obtain a more accurate description of the bandgap and electronic structure.

Acknowledgements

The authors would like to thank the National Supercomputing Laboratory of Southeast Mexico (LNS), part of the SECIHTI national laboratory network, for the computational resources, support, and technical assistance provided through project No. 202503043N. Similarly, the authors thank SECIHTI for the financial support provided to R. Flores-Cruz in the doctoral programme (432) in the Academic Area of Earth and Materials Sciences and the Institute of Basic Sciences and Engineering at the Autonomous University of the State of Hidalgo. Finally, the authors acknowledge CITNOVA for the Postdoctoral Fellowship awarded to Dr. J. Ortega-Lazcano and the support for R. Flores-Cruz international research stay at UPV.

References

Aliabad, H. A. R., & Kheirabadi, M. (2013). Electronic and structural properties of Sb_2Te_3. Physica B: Condensed Matter, 433, 157-161. https://doi.org/10.1016/j.physb.2013.10.035

Chen, Y. L., Analytis, J. G., Chu, J.-H., Liu, Z. K., Mo, S.-K., Qi, X. L., Zhang, H. J., Lu, D. H., Dai, X., Fang, Z., Zhang, S. C., Fisher, I. R., Hussain, Z., & Shen, Z.-X. (2009). Experimental realization of a three-dimensional topological insulator, Bi_2Te_3. Science, 325(5937), 178-181. https://doi.org/10.1126/science.1173034

Dudarev, S. L., Botton, G. A., Savrasov, S. Y., Humphreys, C. J., & Sutton, A. P. (1998). Electron-energy-loss spectra and the structural stability of nickel oxide. Physical Review B, 57, 1505-1509. https://doi.org/10.1103/PhysRevB.57.1505

Fang, T., Li, X., Hu, C., Zhang, Q., Yang, J., Zhang, W., Zhao, X., Singh, D. J., & Zhu, T. (2019). Thermoelectric properties of topological materials. Advanced Functional Materials, 29. https://doi.org/10.1002/adfm.201900677

Gong, Y., Guo, J., Li, J., Zhu, K., Liao, M., Liu, X., Zhang, Q., Gu, L., Tang, L., Feng, X., Zhang, D., Li, W., Song, C., Wang, L., Yu, P., Chen, X., Wang, Y., Yao, H., Duan, W., et al. (2019). Experimental realization of magnetic topological insulators. Chinese Physics Letters, 36, 076801. https://doi.org/10.1088/0256-307X/36/7/076801

Hasan, M. Z., & Kane, C. L. (2010). Colloquium: Topological insulators. Reviews of Modern Physics, 82(4), 3045-3067. https://doi.org/10.1103/RevModPhys.82.3045

Larson, P., Greanya, V. A., Tonjes, W. C., Liu, R., Mahanti, S. D., & Olson, C. G. (2002). Electronic structure of Sb_2Te_3. Physical Review B, 65, 085108. https://doi.org/10.1103/PhysRevB.65.085108

Larson, P., Mahanti, S. D., & Kanatzidis, M. G. (2000). Electronic structure of Sb_2Te_3 and related compounds. Physical Review B, 61, 8162-8167. https://doi.org/10.1103/PhysRevB.61.8162

Lawal, A., & Shaari, A. (2017). Electronic properties of topological insulators. Malaysian Journal of Fundamental and Applied Sciences, 12.

Lee, D. S., Kim, T.-H., Park, C.-H., Chung, C.-Y., Lim, Y. S., Seo, W.-S., & Park, H.-H. (2013). Crystal growth and characterization of topological insulator materials. CrystEngComm, 15, 5532-5538. https://doi.org/10.1039/C3CE40643A

Li, J., Li, Y., Du, S., Wang, Z., Gu, B.-L., Zhang, S.-C., He, K., Duan, W., & Xu, Y. (2019). Intrinsic magnetic topological insulators in van der Waals layered materials. Science Advances, 5. https://doi.org/10.1126/sciadv.aaw5685

Li, S., Liu, T., Liu, C., Wang, Y., Lu, H.-Z., & Xie, X. C. (2023). Topological materials and their applications. National Science Review, 11. https://doi.org/10.1093/nsr/nwac296

Michiardi, M., Aguilera, I., Bianchi, M., De Carvalho, V. E., Ladeira, L. O., Teixeira, N. G., Soares, E. A., Friedrich, C., Blügel, S., & Hofmann, P. (2014). Bulk band structure of topological insulators. Physical Review B, 90, 075105. https://doi.org/10.1103/PhysRevB.90.075105

Mishra, S. K., Satpathy, S., & Jepsen, O. (1997). Electronic structure and thermoelectric properties of bismuth telluride and antimony telluride. Journal of Physics: Condensed Matter, 9, 461-470. https://doi.org/10.1088/0953-8984/9/2/014

Otrokov, M. M., Rusinov, I. P., Blanco-Rey, M., Hoffmann, M., Vyazovskaya, A. Y., Eremeev, S. V., Ernst, A., Echenique, P. M., Arnau, A., & Chulkov, E. V. (2019). Prediction and observation of magnetic topological insulators. Physical Review Letters, 122, 107202. https://doi.org/10.1103/PhysRevLett.122.107202

Sharma, V., Sharda, S., Sharma, N., Katyal, S. C., & Sharma, P. (2019). Topological insulators: A review. Progress in Solid State Chemistry, 54, 31-43. https://doi.org/10.1016/j.progsolidstchem.2019.04.001

Soler, J. M., Artacho, E., Gale, J. D., García, A., Junquera, J., Ordejón, P., & Sánchez-Portal, D. (2002). The SIESTA method for ab initio order-N materials simulation. Journal of Physics: Condensed Matter, 14, 2745-2779. https://doi.org/10.1088/0953-8984/14/11/302

Thouless, D. J., Kohmoto, M., Nightingale, M. P., & Nijs, M. den. (1982). Quantized Hall conductance in a two-dimensional periodic potential. Physical Review Letters, 49(6), 405-408. https://doi.org/10.1103/PhysRevLett.49.405

Tian, W., Yu, W., Shi, J., & Wang, Y. (2017). The properties and applications of topological insulators: A review. Materials, 10(7), 814. https://doi.org/10.3390/ma10070814

Trang, C. X., Li, Q., Yin, Y., Hwang, J., Akhgar, G., Di Bernardo, I., Grubišić-Čabo, A., Tadich, A., Fuhrer, M. S., Mo, S.-K., Medhekar, N. V., & Edmonds, M. T. (2021). Electronic structure of topological materials. ACS Nano, 15, 13444-13452. https://doi.org/10.1021/acsnano.1c03936

Wang, K. L., Lang, M., & Kou, X. (2015). Spintronics of topological insulators. En Spintronics of Topological Insulators (p. 431). Springer. https://doi.org/10.1007/978-94-007-6892-5_56

Zhang, H., Liu, C.-X., Qi, X.-L., Dai, X., Fang, Z., & Zhang, S.-C. (2009). Topological insulators in Bi_2Se_3, Bi_2Te_3 and Sb_2Te_3. Nature Physics, 5, 438-442. https://doi.org/10.1038/nphys1270

Zhou, G., & Wang, D. (2015). Electronic properties of topological insulators. Scientific Reports, 5, 8099. https://doi.org/10.1038/srep08099